Turkish Computational and Theoretical Chemistry

Turkish Comp Theo Chem (TC&TC)

Volume(Issue): 6(1) – Year: 2022 – Pages: 52-65

e-ISSN: 2602-3237

https://doi.org/10.33435/tcandtc.1029382

Received: 17.10.2021 ***Accepted:*** 20.12.2021 *Research Article*

Computational investigation of the synthesized new indoline-2,3-dione and their derivatives

Nazli Afshar[a], Abolfazl Shiroudi[b,1], Farhad Hatamjafari[a,2], Ahmad Reza Oliaey[a], Khalil Pourshamsian[a]

[a]Chemistry Department, Tonekabon Branch, Islamic Azad University, Tonekabon, Iran
[b]Young Researchers and Elite Club, East Tehran Branch, Islamic Azad University, Tehran, Iran

Abstract: Computational studies using DFT incorporating the B3LYP/6-311++G(d,p) level is used to predict the stability of the synthesized 1-(5-phenyl-4*H*-1,2,4-triazol-3-yl)indoline-2,3-dione and its *para*-substituted (X: $-CH_3$, –F, –CN, $-NO_2$) in different solvents (acetone, ethanol, and methanol) and gas phases. Energetic properties, atomic charges, dipole moments, natural bond orbital (NBO), molecular electrostatic potential (MEP), and frontier molecular orbital (FMO) analyses are studied. The gauge independent atomic orbital (GIAO) method is used to quantify the nuclear magnetic resonance (NMR) chemical shift of the molecules. NBO analysis was used to assess the stability of the considered molecules, as well as their hyperconjugative relationships and electron delocalization. The charge transfer within the molecules is determined using the HOMO and LUMO analyses. The MEP surface was performed by the DFT method to predict the reactive sites for nucleophilic and electrophilic attacks. FMO analysis revealed that compound **5** (X=NO_2) has a lower HOMO-LUMO energy (E_{H-L}) gaps in the considered phases, and is thus kinetically more stable in different media. Chemical reactivity indices as NO_2 > CN > Cl > H > CH_3 that predict the lowest (X=CH_3) and highest (X=NO_2) activity for the studied compounds. The energy difference derived from E_{H-L} gap leads to intramolecular hyperconjugative interactions $\pi \rightarrow \pi^*$.

Keywords: 1,2,4-triazole; substituent/solvent effects; DFT; PCM; NBO; HOMO-LUMO gap

1. Introduction

Triazoles are the most well-known medicinal moieties in which carbon atoms are isosterically substituted by nitrogen atoms [1]. Because of their medicinal and industrial properties, triazole chemistry plays an important role in the pharmaceutical industry [2]. The 1,2,4-triazole scaffolds have gotten a lot of attention as chemotherapeutic agents because of their disparate biological properties [3]. The synthesis of indole derivatives has received a lot of attention, and the findings show that the majority of them have a lot of pharmacological activity [4–6]. Indoles have the potential to be used in the manufacture of medicines for the treatment of cancer, bacterial infections, inflammation, and other diseases. Triazole is known to be a pharmacologically significant nucleus, and the triazolic nucleus is actually considered an important component of bioactive compounds in design and synthesis. Derivatives 1,2,4-triazole due to their attractive structural properties such as simple accessibility, the role of nitrogen atoms as hydrogen bonds acceptors, the involvement of heterocyclic π-conjugated system and aromatic systems with a wide range of biological activities namely antibacterial, antimicrobial, anticancer, anti-HIV, anti-inflammatory, analgesic, anticonvulsant, antidiabetic, antihistaminic, anti-allergic, antidepressant, anti-hypertensive, anti-parasitic, estrogen receptor modulating agents, sedatives, cardio tonics and anti-asthma and so on [7]. The

Corresponding Authors
e-mail: [1]abolfazl.shiroudi@iauet.ac.ir, [2]hatamjafari@yahoo.com

chemical reactivity of 1,2,4-triazoles is determined by the nucleophile, the incremental commodity stability of the transition state, the selectivity site, and the dielectric constant of the most widely utilized solvent [8].

In preceding studies the characteristics of triazole compounds have been investigated [9]. 1,2,4-triazole rings are usually planar 6π-electron aromatic structures. Aromaticity is the main reason of stability of triazole nucleus [10,11]. The aromaticity and rich electron properties of triazole make it possible to bind to various types of enzymes and receptors by interactions such as ion-dipole, coordination bonds, hydrophobic effects, and make them commonly used in the variety fields [12]. Density functional theory (DFT) method is used to measure the molecular structure and energy of molecules. The self-consistent reaction field (SCRF) model is one of the implicit solvent purification molecules that use the continuous polar model (PCM). This model is the first SCRF approach used in DFT, and it is a reasonable way to investigate the influence of solvents [13]. Changes in the molecular composition alter the distribution of electrons within a molecule specifically responsible for molecular activity [14]. This alteration is also responsible for improvements in descriptor values or physico-chemical properties [15]. The knowledge of the charge distribution on different atoms in molecules is helpful in determining possible active sites because it provides important knowledge of hydrogen bonding ability, electrophilic attack sites, and molecular reactivity studies that are known using molecular electrostatic potential (MEP) mapping [16]. The study of molecular orbitals reveals information about the presence of electrophiles, electronegativity, hardness, and reactivity [17].

To our knowledge, there have been no other theoretical calculations for the solvent and substituent effects of 1-(5-phenyl-4H-1,2,4-triazol-3-yl)indoline-2,3-dione and its derivatives (X: CH_3, F, CN, and NO_2) in the considered solvent (ethanol, methanol, and acetone) and gas phases. Thus, we present quantum chemical investigations on the energetic parameters of the studied forms, as well as using PCM at the B3LYP/6-311++G(d,p) theoretical level [18,19] to determine those properties in the studied solvents (methanol, ethanol, and acetone), and comparing them to the same properties in the gas phase. The behavior of the studied forms and their relative stabilities in different media are analyzed in order to gain a thorough understanding of the influence of substituents and solvents on molecular properties. The dipole moment of the molecules under consideration is also computed using the same method and basis set. Moreover, NBO analysis [20] was used to measure the redistribution of electron density (ED) in various bonding and antibonding orbitals, as well as $E(2)$ energies, in order to provide clear evidence of stabilization resulting from the hyperconjugation of various intramolecular interactions. The calculated LUMO, HOMO, and molecular electrostatic potential maps (MEP) of the considered compounds provide detailed explanations of their molecular electronic properties. These are confirming the charge transfer within the molecule. Similarly the nuclear magnetic resonance (NMR) chemical shift [21-25] of the molecules are measured at the same theoretical level using the gauge independent atomic orbital (GIAO) method [26,27]. As a final point, we use nucleus-independent chemical shift (NICS) techniques to validate our findings [21,22,25].

2. Computational Method

All of the quantum chemistry calculations were carried out using the Gaussian 09 program [28,29]. The geometry optimization of the investigated molecules were performed using the DFT method with the B3LYP functional and the 6-311++G(d,p) basis set in the gas-phase and various media. The optimized structures were also confirmed to be real minima by frequency calculations. Atomic charges, frontier molecular orbitals (FMO) properties, natural bond orbital (NBO) analysis, dipole moments, and second perturbation stability are measured using the NBO technique. The molecular properties such as electronegativity (χ), chemical potential, ionization potential (IP), chemical hardness (η) and softness (ζ) and global electrophilicity index (ψ) were calculated using HOMO-LUMO analysis at the B3LYP/6-311++G(d,p) level of theory. The effect of solvents on the relative stability and geometry of the studied forms is investigated using the SCRF approach based on the PCM [30–32] in the gas phase and solvent under consideration. The aromaticity index NICS values were measured using the GIAO

method in various media at the same theoretical level. As a final point, to approximate the influence of the liquid environment, the geometries of the considered compounds were re-optimized in solvents *i.e.,* polar protic [ethanol (ε=24.55) and methanol (ε=33.00)], and polar aprotic [acetone (ε=20.7)] at a P=1 atm and ambient temperature.

3. Results and discussion

The synthesis of form **A**, *N*-(9-oxo-9*H*-[1,2,4]triazolo[4,3-*a*]indol-3-yl)benzamide (**2*a–e***) and form **B**, 1-(5-phenyl-4*H*-1,2,4-triazol-3-yl)indoline-2,3-dione (**3*a–e***) and their derivatives were performed by reaction of different synthesized *N*-(2,3-dioxoindoline-1-carbonothioyl) benzamide derivatives (**1*a–e***) with hydrazine hydrate solution (**2**). The optimized structures of forms **A** and **B** were investigated in details, as seen in Scheme 1.

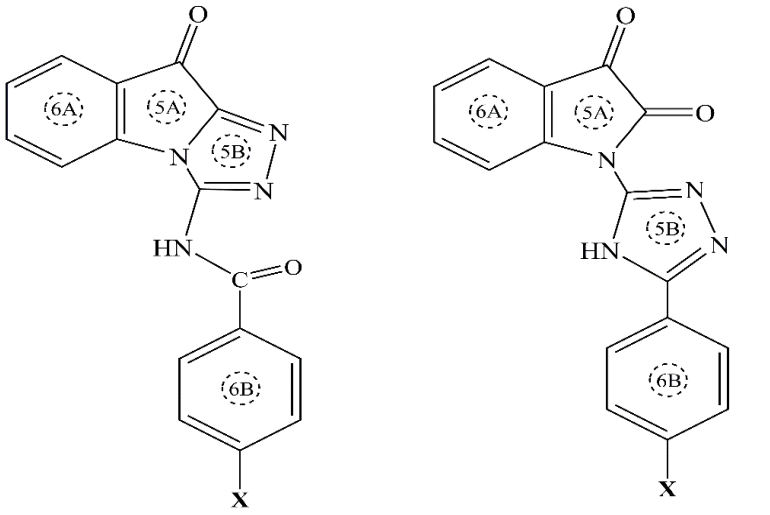

form **A** (Non-linear) form **B** (linear)

Scheme 1. The synthesis of the studied compounds.

3.1. Energy and thermodynamic parameters

Structures and numbering of the 1-(5-phenyl-4*H*-1,2,4-triazol-3-yl) indoline-2,3-dione and its *para*-derivatives are shown in Scheme 1. The sum of electronic and zero-point energies (E_A or E_B) and relative energy (ΔE) were studied in gas phase and various solvents at T=298.15 K, and are summarized in Table 1.

As shown in Table 1, the relative energy stability orders for the studied forms in both phases as: form **B** > form **A**. The finding results indicate that an increase in the stability of the electron withdrawing groups in the form **B**. In the analyzed solvents and gas phase, forms **B** are approximately 11.92–15.68 and 15.22–17.19 kcal mol^{-1}, respectively more stable than forms **A**. The nitro derivative (X=NO_2) with 17.19 kcal mol^{-1} has the largest difference between the two forms in the gas phase. The calculations in the presence of the chosen solvents revealed that acetone further stabilizes forms **B** of the other forms (**A**).

3.2. Dipole moments

Dipole moments (μ) vary significantly in the transition from the gas phase to the solvent, and their major values in the solvent phase can be explained by interactions with the dipole moment of the compound and the solvent molecules [33]. The experimental μ is not known in this work. The calculated dipole moments for the considered forms in various environments are summarized in Table 2. The dipole moments for all forms **A** are increased by changing the environment from the gas phase to the selected solvents implying an increase in the observed solute-solvent interaction (Table 2). It is clear that the most important difference between the μ values of forms A and B with the CH_3 substituent is ~8.94 D in acetone. The largest μ obtained for all molecules (**A** and **B**) was found in methanol solvents, and in methanol solvent, the most obtained dipole moment for form **B** is observed.

Table 1. Total energies (Hartree), and relative energies, ΔE (kcal mol^{-1}) for series of the 1,2,4-triazole derivatives form **A** (*non-linear*) and form **B** (*linear*) in gas phase and solvents. (P=1 atm, T=298 K)

Substituent	Structure form	Gas (ε=1.00)	Acetone (ε=20.70)	Ethanol (ε=24.55)	Methanol (ε=33.00)
$-CH_3$	E_A	−1024.47736	−1024.51894	−1024.51444	−1024.51341
	E_B	−1024.50161	−1024.54129	−1024.53388	−1024.53243
	ΔE_{A-B}	15.222	14.024	12.198	11.938
−H	E_A	−985.175778	−985.21714	−985.21252	−985.21155
	E_B	−985.200689	−985.23966	−985.23233	−985.23054
	ΔE_{A-B}	15.632	14.133	12.432	11.915
−F	E_A	−1084.45238	−1084.49400	−1084.48948	−1084.48852
	E_B	−1084.47710	−1084.51656	−1084.50943	−1084.50759
	ΔE_{A-B}	15.510	14.155	12.518	11.970
−CN	E_A	−1077.44039	−1077.48720	−1077.48164	−1077.48054
	E_B	−1077.46720	−1077.51133	−1077.50326	−1077.50141
	ΔE_{A-B}	16.820	15.141	13.564	13.091
$-NO_2$	E_A	−1189.73284	−1189.77941	−1189.77256	−1189.77092
	E_B	−1189.76024	−1189.80440	−1189.79551	−1189.79326
	ΔE_{A-B}	17.191	15.681	14.401	14.017

E_A,E_B: Sum of electronic and zero-point energies (E_{elec}+ZPE)

Because of their greater dipole moments, the considered forms A are more stable in solution than in vacuum (Table 2). In the gas phase, the measured dipole moments of form **A** for the –H, $-CH_3$, –F, –CN and $-NO_2$ substituents are large (6.46, 6.76, 6.00, 6.61, and 6.74 D, respectively), but they decrease considerably when moving to the other form (1.39, 1.33, 2.56, 6.20, and 6.72 D, respectively). As a result, forms **A** would have a significant interaction with polar solvents.

Table 2. Calculated dipole moment of optimized forms (in Debye) in gas phase and solvents.

Compound / *Debye*	Structure	Gas (ε=1.00)	Acetone (ε=20.70)	Ethanol (ε=24.55)	Methanol (ε=33.00)
–H	A	6.4619	9.1907	9.3729	9.4764
	B	1.3919	1.0146	1.5495	1.6602
$-CH_3$	A	6.7557	9.8840	10.1216	10.2109
	B	1.3301	0.9407	1.5027	1.5227
–F	A	6.0024	8.7979	8.8230	8.8850
	B	2.5546	3.0821	3.3680	3.4515
–CN	A	6.6133	9.1044	9.1919	9.2460
	B	6.2005	7.7226	7.8670	7.9386
$-NO_2$	A	6.7345	9.9278	9.6434	9.7215
	B	6.7176	8.1848	8.9474	9.1180

3.3. Solvent effects

Since polarity variations between forms can induce important changes in their relative energies in solution, solvent effects are significant in stability phenomena [34]. General properties of solvents include polarity, solubility and polarization parameters, refractive index, dielectric constant (relative permittivity) and more precise properties such as Lewis or Bronsted basicity or acidity and H-bonding ability (donor or acceptor). The PCM measurements are used to determine the solvent effects on the molecules under consideration. It is worth noting that the PCM model does not take clear solvent molecules into account; thus, specific solute-solvent interactions are not specified and the solvation results under consideration arise only from mutual solute-solvent electrostatic polarization. Aqueous solution calculations yield the lowest energy values for the studied forms. The polarity of the studied solvents was improved by reducing the energy variations between the investigated forms of substituents (Table 1).

The dipole moments of form **A** with the X=H, CH_3, F, CN derivatives and form **B** with the X=F, CN,

NO_2 derivatives are increased with increasing polarity of the medium (see Table 2). In addition, the variations in dipole moments in the considered solvents are marginal for the studied form **A** with fluorine substituent, but the studied groups (X= H, CH_3, F) raise the dipole moments of forms **A** over forms **B**. In the presence of a solvent field, the charge distributions of dipolar forms are often significantly changed. By using the NBO technique, we investigated the charge distribution for the considered forms in solvent and gas phases. The charge distribution differs differently with increasing polarity for any atom in the solvents, for example, a regular increase in negative charge was discovered for the N7 atom in form **B** derivatives when passing from gas phase to a more polar solvent (Table 2). The charge distribution on the N7 is influenced by the polarity of solvents as well as the nature of the substituent.

3.4. Nucleus independent chemical shift (NICS) analysis

The magnetic criterion of aromaticity is the NICS index, which is estimated using absolute magnetic shielding. The NICS values determined as the negative shielding constant at the center as well as above and below geometric center of the ring [35,36]. For all structures analyzed, all points below and above the geometric centers of the ring (–1.5 to 1.5 Å with 0.5 Å steps) were used. Because all species' NICS plots were nearly symmetrical along the molecule plane, we only show the points above the plane in Fig. 1. The minima NICS values for the forms **A** and **B** in the gas phase influenced consistent with the existence of the delocalized π-system structures were located at the distance of 0.5 Å and 1 Å above and below the plane, respectively (Fig. 1).

The obtained results show that the magnitudes of the aromaticity characters agree with the stabilization energy, implying that these patterns are influenced by changes in aromaticity in various media. The studied forms show that NICS values for form **A** decreases from the NICS(±1) point located at the ring to 1.5 Å below/above, while for form **B** will decrease from ±0.5 to ±1.5 Å, which is consistent with the presence of delocalized π-electron current below/above the molecule plane, and thus a decrease in aromaticity is expected (Table S1 in the Supplementary material). Furthermore, the lower energy of form **B** with different substituents compared with the other form reflects the greater aromaticity: indeed, forms **A** and **B** are characterized by NICS indices ranges as follows:

- forms **A**: NICS(0)=(−4.963)–(−6.449)], and NICS(+1)=(−20.704)–(−21.667)
- forms **B**: NICS(0)= (−22.394)–(−23.892), and NICS(±0.5)=(−26.911)–(−28.021)

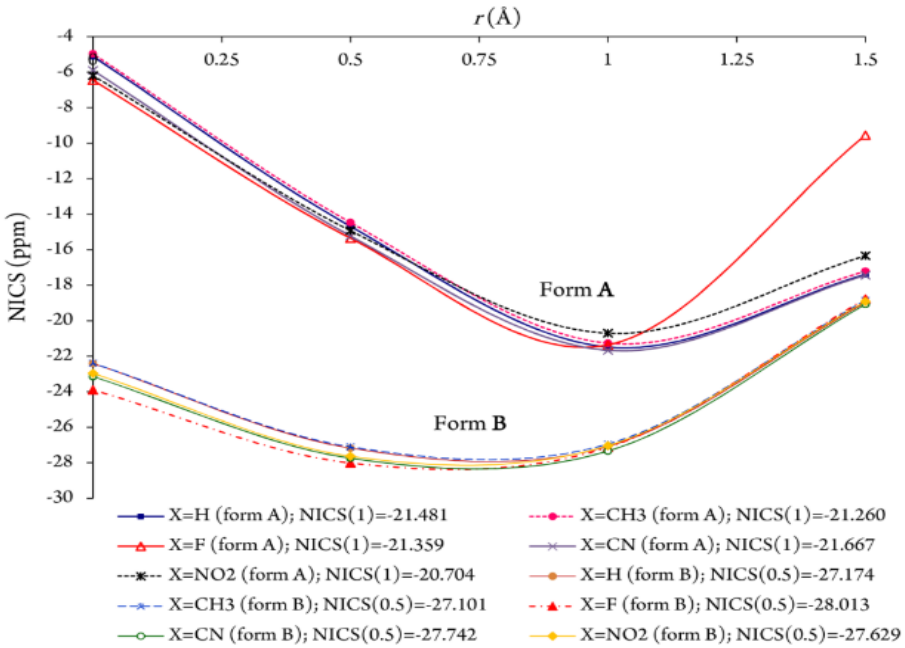

Figure 1. Aromaticity of the all studied forms versus distance from the ring geometric center up to 1.5 Å above the ring

As shown in Fig. 1, the maximum total diatropic current is observed at 1 Å above the molecule's geometric center in form **A**, and at 0.5 Å above/below the rings in form **B**. Interestingly, NICS values at the minimal point of six-membered rings are more negative than those of five-membered rings for all studied forms. Because form **B** is more negative and aromatic than forms **A**, NICS findings indicated that the order of aromaticity in the gas phase and solvents were form **B** > form **A** (see Fig. 1 and Table S1 of the Supplementary material). As a result, in the following sections, we will only look at the more stable form [form **B**]. For the more stabilized form in this work, the maximum NICS(±1) values of the compound **1** (X=CH_3) in the considered media calculated to be in the ranges of (−23.868)–(−26.945) ppm, while the NICS values of the compound **5** (X=NO_2) give the highest NICS(±1) value ranging from −23.415 to −27.037 ppm (see Table S1 of the Supplementary material). The aromaticity of the compounds **1**–**5** changes with differing dielectric constant of the media for points located at the center of the six- and five-membered rings, as well as points located at 1.5 Å above and below the ring centers (see Fig. 2). The data confirms that aromaticity of forms **B** changes with differing dielectric constant of the media for points located at the center of the six- and five-membered rings, as well as points located at 1 Å above/below the ring centers. The NICS value for five-membered ring [**5A**] of all forms **B** are positive, indicating that the **5A** rings are antiaromatic, while the NICS values for other rings are negative, and indicates the presence of π-aromaticity.

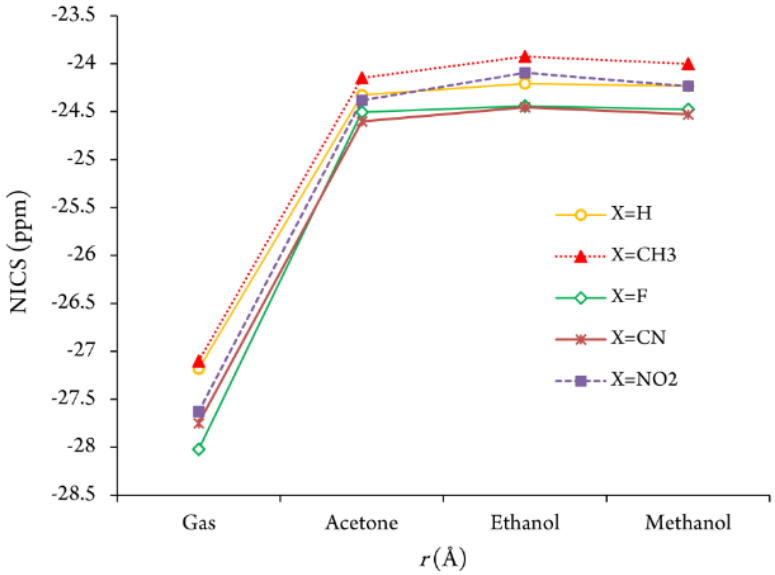

Figure 2. Overall aromaticity of all forms **B** estimated as a function of NICS *versus* distance from ring geometric center. NICS values at maximum diatropic current are tabulated.

3.5. Natural population analysis (NPA) atomic charges

Atomic charges on numerous molecular atoms are very useful for detection and possible active sites. Excessive charge is important in a molecule's interaction with a charge depletion receptor site. Calculation of NPA charges plays a key role as atomic charges induce dipole moment, electronic structure, and molecular reactivity of various molecular properties [37]. We investigated the charge distributions in various media using NBO techniques at the B3LYP/6-311++G(d,p) level, which is detailed in Table S2 of the Supplementary material. In the case of benzene rings, all carbon atoms are expected to be negative, but the C4 atom is found to be positively charged. All hydrogen atoms are found to be as positive as predicted, as are for other hydrogen atoms.

The nitrogen atom (N13) in the five-membered ring (**5B**) and the oxygen atom (O10) attached to the five-membered ring (**5A**) have more negative charges (see Fig. 3 and Table S2 in the

Supplementary material). When compared to other atoms, C8, C9, C12, and C14 have the highest positive atomic charge. This is caused by the attachment of negatively charged (O10, O11, N7, N13) atoms. Furthermore, the result implies that all atoms bonded to the nitrogen N13 atom (H27, C12, C14) are electron acceptors and that charge transfer from them (H27, C12, C14) to the nitrogen atoms occurs (N7, N13, N15, N16). The electronic effect caused by the hyperconjugation and induction of the studied substituents in the six-membered ring (**6B**) results in a significant negatively charged value on the carbon atom C20 (see Table S2 in the Supplementary material).

The charges at this H-site (H27 atom) are estimated to be 0.4514e (X=H), 0.4509e (X=CH_3), 0.4514e (X=F), 0.4533e (X=CN), and 0.4537e (X=NO_2). The sequence of the NH hydrogen charge density of the triazole ring is NO_2 > CN > F > H > CH_3. This order corresponds to the chemical sense in which the electron releasing substituent, *i.e.* the methyl group (compound **1**), reduces the positive charge at this H-site, while the nitro substituted derivative (compound **5**) has the largest positive NH proton. The atomic charge for this nitrogen (N13) associated with the N13–H27 bond is within the range of –0.5584e to –0.5626e for compounds **1**–**5**. As illustrated in Table S2 of the Supplementary material, compound **5** (X=NO_2) demonstrated a high positive value of the hydrogen atom (H27) associated with the nitro substituted of 0.4537e as a result of its bonding to the six-membered ring that is connected to the triazole ring.

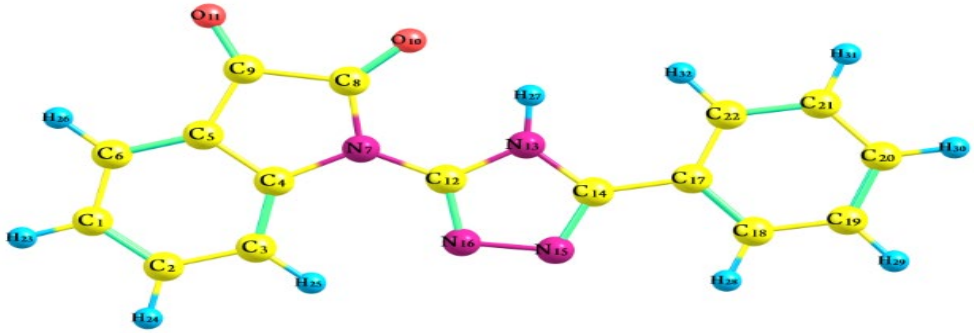

Figure 3. Optimized geometrical compound structure (X=H) along with atom numbering scheme.

Moreover, except for those atoms attached to the strong electronegative oxygen and nitrogen atoms, carbon atoms C4, C8, C9, C12, and C14 are negatively charged (see Fig. S1 and Table S2 in the Supplementary material). Carbon atomic charges (C20) in six-membered of compounds **1–5** are –0.1919e (X=H), –0.0181e (X=CH_3), 0.4197e (X=F), –0.1750e (X=CN), and 0.0745e (X=NO_2), respectively. The carbon atom of the C–F bond in compound **3** has the most positive charge of 0.4197e than the carbon atom of the C–H bond in compound **2** (X=H) (–0.1919e), which corresponds to the fluorine atom's higher electronegative nature (–0.3494e) when compared to the H atom (0.2073e). So, the attached carbon atom, C20 in compound **3** is found the most positive aromatic carbon atom.

3.6. FMO and global reactivity descriptors

The frontier electron density uses molecular orbitals to predict the most reactive position in π-electron systems, and it also describes several types of reactions in the conjugated system. During molecular interactions between LUMO and HOMO, the LUMO accepts electrons and its energy is associated with the electron affinity (EA), while the HOMO (electrons donor) energy is related to the ionization potential (IP) [33].

A molecule with a small HOMO-LUMO gap, low kinetic stability, and high chemical reactivity is referred to as a soft molecule, because adding an electron to the high-lying LUMO in order to remove electrons from the low-lying HOMO is energetically unfavorable [38]. The global electrophilicity index (ω) is characterized as the decrease in energy caused by electron flow from the HOMO to LUMO in molecules. It also plays an important role in determining the chemical reactivity of a system as $\omega = \mu^2/2\eta$, where μ is the electronic chemical potential which defines charge transfer [$\mu=(E_{LUMO}+E_{HOMO})/2$], and η denotes the global chemical hardness [$\eta=(E_{LUMO}-E_{HOMO})/2$] within a system. Moreover, S is the global softness

[$S=1/\eta$], ΔN_{max} represents maximum electronic charge [$\Delta N_{max}= -\mu/\eta$], and χ is the absolute electronegativity [χ=(IP+EA)/2], which is used to compute the electron transfer direction [33].

The properties of FMOs are also examined in order to better understand the global reactivity of the studied molecules in all considered media. The $E_{HOMO-LUMO}$ (E_{H-L}) energy gap is increasing from the CH_3 group to the NO_2 derivatives as follows: NO_2 > CN > F > H > CH_3. As seen in Table 3, compounds with a methyl substituent are the least stable species in the gas phase and solvents; thus, the reactivity of the 1,2,4-triazole ring is increased by this substituent. The highest E_{H-L} gap is obtained with the nitro substituent, which reduces the reactivity of the five-membered ring. Thus, the stability of the investigated compounds is as **1** (CH_3) < **2** (H) < **3** (F) < **4** (CN) < **5** (NO_2). Compounds with a higher chemical potential are more reactive than those with a lower electronic chemical potential. In the studied media, compound **5** is harder and more stable (less reactive), whereas compound **1** is softer and less stable (more reactive).

Likewise, compound **5** has a higher electronegativity and exhibits a high charge flow. Also, compound **1** has the lowest IP and thus is the most nucleophilic, while compound **5** is highly electrophilic. All compounds in various media have a positive ΔN_{max} and function as electron acceptors (Table 3).

Table 3. Calculated global reactivity descriptors of the stable form (form B) and its derivatives.

Parameter / Substituent	HOMO / a.u.	LUMO / a.u.	ΔE / eV	μ / eV	η / eV	ω / eV	S / (eV)$^{-1}$	χ / eV	ΔN_{max}	IP / eV	EA / eV
	Gas (ε=1.00)										
CH_3	–0.2318	–0.1255	2.894	–4.861	1.447	222.142	9.402	4.861	91.402	6.308	3.414
H	–0.2368	–0.1268	2.994	–4.947	1.485	222.425	9.088	4.947	89.918	6.444	3.450
F	–0.2391	–0.1290	2.995	–5.008	1.497	227.882	9.087	5.008	91.010	6.505	3.511
CN	–0.2517	–0.1363	3.140	–5.280	1.570	241.564	8.666	5.280	91.505	6.850	3.710
NO_2	–0.2547	–0.1363	3.222	–5.319	1.611	238.918	8.445	5.319	89.838	6.930	3.708
	Acetone (ε=20.70)										
CH_3	–0.2322	–0.1256	2.901	–4.868	1.450	222.312	9.381	4.868	91.334	6.318	3.418
H	–0.2369	–0.1273	2.986	–4.956	1.493	223.827	9.113	4.956	90.328	6.449	3.463
F	–0.2395	–0.1293	2.999	–5.017	1.500	228.384	9.073	5.017	91.040	6.517	3.518
CN	–0.2506	–0.1347	3.153	–5.242	1.576	237.145	8.631	5.242	90.484	6.818	3.665
NO_2	–0.2553	–0.1363	3.238	–5.328	1.619	238.517	8.403	5.328	89.536	6.947	3.709
	Ethanol (ε=24.55)										
CH_3	–0.2323	–0.1259	2.896	–4.873	1.448	223.094	9.395	4.873	91.563	6.321	3.425
H	–0.2372	–0.1274	2.989	–4.960	1.495	223.968	9.102	4.960	90.303	6.455	3.466
F	–0.2398	–0.1293	3.007	–5.023	1.503	228.325	9.050	5.023	90.913	6.526	3.520
CN	–0.2509	–0.1347	3.161	–5.246	1.581	236.909	8.607	5.246	90.314	6.827	3.666
NO_2	–0.2556	–0.1367	3.237	–5.338	1.619	239.483	8.406	5.338	89.736	6.956	3.719
	Methanol (ε=33.00)										
CH_3	–0.2322	–0.1259	2.891	–4.872	1.446	223.348	9.411	4.872	91.693	6.317	3.426
H	–0.2373	–0.1274	2.992	–4.961	1.496	223.878	9.096	4.961	90.252	6.457	3.465
F	–0.2399	–0.1294	3.006	–5.025	1.503	228.540	9.051	5.025	90.964	6.528	3.522
CN	–0.2509	–0.1348	3.161	–5.249	1.581	237.139	8.608	5.249	90.362	6.829	3.668
NO_2	–0.2557	–0.1367	3.238	–5.340	1.619	239.606	8.404	5.340	89.748	6.958	3.721

The energies of four important MOs for all forms **B** in the gas phase, as well as pictorial representations of these frontier orbitals; the 2nd lowest unoccupied MO's (LUMO and LUMO+1) and the 2nd highest and highest occupied MOs (HOMO and HOMO−1)

explored at the B3LYP/6-311++G(d,p) level, and are shown in Fig. S2 of the Supplementary material. According to natural population analysis, these frontier molecular orbitals are primarily composed of *p* atomic orbitals, as seen by the shapes of HOMO and LUMO orbitals in Fig. S2 of the Supplementary material, and hence the electronic transitions are primarily derived from the contributions of bands $\pi\rightarrow\pi^*$. The HOMO−1 of the studied compounds in the gas phase is mainly delocalized among the atoms of the five-membered ring (**5A**), whereas LUMOs are partly or mainly delocalized among the atoms of the largest *p*-electronic conjugated portions [rings of **5A** and **6A**] and HOMOs are principally delocalized among the atoms of the all five and six-membered rings (**5A**, **5B**, **6A**, and **6B**). However, their LUMO+1s are mainly or partly delocalized among the molecules' terminals (**5B** and **6B**).

3.7. Molecular electrostatic potential

The electron density is associated with the molecular electrostatic potential, which is a very useful descriptor in understanding possible sites for hydrogen bonding interactions and nucleophilic and electrophilic reactions [39]. The various electrostatic potential values at the MEP surface are characterized on the surface by different colors in the order of *red* < *orange* < *yellow* < *green* < *blue*. The negative MEP associated with a proton's attraction by the aggregate electron density (shades of red and yellow), and the positive MEP refers to a proton's repulsion by the atomic nuclei (shade of blue) in the molecule [33]. Molecular electrostatic potential surface of compound **1** (R=H) was identified in Fig. 4. The positive regions (*blue*) are mainly localized around the hydrogen atoms consistent with the benzene rings (**6A** and **6B** rings) and the hydrogen atom (H27) bonded to the 1,2,4-triazole ring (**5B** ring) that are the most reactive sites for a nucleophilic attack, while the negative regions (*red*) are clearly localized over the N15 and N16 atoms that are the most reactive sites for an electrophilic attack (covers the C14–N15 and C12–N16 groups). The electrostatic potential contour diagram confirms the molecule's separate negative and positive potential locations in line with the overall electron density surface map.

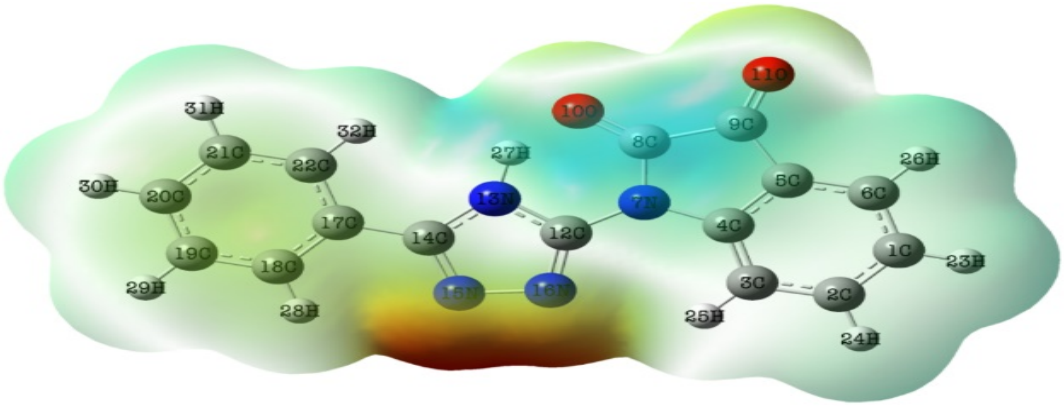

Figure 4. Molecular electrostatic potential plot of the investigated molecule (X=H).

3.8. Natural bond orbital analysis

It expects delocalization or hyperconjugation by taking into account the various 2nd order perturbation energies (E_2) between the filled orbitals of one subsystem and the empty orbitals of another subsystem [33]. The stabilization energy (E_2) related to the delocalization $i\rightarrow j$ for each donor NBO(i) and acceptor NBO(j) in the NBO analysis is given by [40]

$$E_2=\Delta E_{ij}=q_i\left[F^2_{(i,j)}/(\varepsilon_i-\varepsilon_j)\right]$$

where $F_{(i,j)}$ denotes the off-diagonal NBO Fock matrix elements, ε_i and ε_j are diagonal elements (orbital energies), and q_i represents the i^{th} donor orbital occupancy. The $\sigma\rightarrow\sigma^*$ interactions have the lowest delocalization energy relative to the $\pi\rightarrow\pi^*$ interactions (Table 4). Thus, the electron density (ED) of σ bonds is higher than that of π bonds. A strong intramolecular hyperconjugative interaction of the C3–C4 bonds is formed by an orbital overlap between the π_{C3-C4} bonding orbitals and the π^*_{C1-C2} antibonding orbitals with an increasing ED of

0.3145 results in a stabilizing energy of up to 22.51 kcal mol^{-1}, resulting in intramolecular charge transfer, and molecule stabilization. Similarly strong $\pi\rightarrow\pi^*$ interactions occur between the π_{C5-C6} bonding orbital, and the π^*_{C1-C2} , and π^*_{C9-O11} antibonding orbitals, resulting in the corresponding bonds being stabilized by up to 20.23 kcal mol^{-1} [$\pi_{C5-C6}\rightarrow\pi^*_{C1-C2}$], and 22.03 kcal mol^{-1} [$\pi_{C5-C6}\rightarrow\pi^*_{C9-O11}$], respectively, whereas the small $\pi\rightarrow\pi^*$ interaction between bonding $\pi_{N12-C16}$ and antibonding orbitals $\pi^*_{C14-N15}$ that the respective bond is stabilized up to 12.85 kcal mol^{-1} [$\pi_{C12-N16}\rightarrow\pi^*_{C14-N15}$] in the studied compounds.

Table 4. Second-order stabilization energy for the most critical charge transfer interactions of the molecules examined in the gas phase. [The ED(*i*) and ED(*j*) values as the energy densities have reported only for the hydrogen substituent (X=H)].

Donor NBO(*i*)	ED(*i*), a.u. (X=H)	Acceptor NBO(*j*)	ED(*j*), a.u. (X=H)	Interaction type	E_2 / kcal mol^{-1}				
					X=H	X=CH_3	X=F	X=CN	X=NO_2
σ_{C3-C4}	1.97522	σ^*_{C4-N7}	0.03575	$\sigma_{C3-C4}\rightarrow\sigma^*_{C4-N7}$	1.53	1.51	1.52	1.45	1.50
		σ^*_{C2-H24}	0.01242	$\sigma_{C3-C4}\rightarrow\sigma^*_{C2-H24}$	2.24	2.00	1.99	1.98	1.97
		σ^*_{C4-C5}	0.02774	$\sigma_{C3-C4}\rightarrow\sigma^*_{C4-C5}$	5.07	8.30	5.10	5.08	5.13
		σ^*_{C5-C9}	0.06643	$\sigma_{C3-C4}\rightarrow\sigma^*_{C5-C9}$	0.84	1.37	1.44	1.46	1.45
		σ^*_{N7-C8}	0.08751	$\sigma_{C3-C4}\rightarrow\sigma^*_{N7-C8}$	2.09	2.64	1.47	1.46	1.46
π_{C3-C4}	1.65187	π^*_{C1-C2}	0.31449	$\pi_{C3-C4}\rightarrow\pi^*_{C1-C2}$	20.23	22.51	21.13	< 0.50	17.78
σ_{C4-C5}	1.96372	σ^*_{C3-C4}	0.02173	$\sigma_{C4-C5}\rightarrow\sigma^*_{C3-C4}$	< 0.50	4.37	4.31	4.13	4.33
		σ^*_{C4-N7}	0.03575	$\sigma_{C4-C5}\rightarrow\sigma^*_{C4-N7}$	0.52	0.51	0.52	< 0.50	0.51
		σ^*_{C5-C6}	0.02280	$\sigma_{C4-C5}\rightarrow\sigma^*_{C5-C6}$	5.81	4.55	4.23	4.03	4.22
		σ^*_{C5-C9}	0.06643	$\sigma_{C4-C5}\rightarrow\sigma^*_{C5-C9}$	1.55	1.18	1.25	1.26	1.26
		σ^*_{C6-H26}	0.01367	$\sigma_{C4-C5}\rightarrow\sigma^*_{C6-H26}$	2.09	2.15	2.10	2.14	2.08
σ_{C4-N7}	1.97934	σ^*_{N7-C8}	0.08751	$\sigma_{C4-N7}\rightarrow\sigma^*_{N7-C8}$	3.06	0.76	1.14	1.10	< 0.50
		$\sigma^*_{C12-N13}$	0.03494	$\sigma_{C4-N7}\rightarrow\sigma^*_{C12-N13}$	3.23	2.17	2.43	2.11	2.48
		σ^*_{C2-C3}	0.01553	$\sigma_{C4-N7}\rightarrow\sigma^*_{C2-C3}$	< 0.50	0.99	0.88	0.98	0.87
		σ^*_{C3-C4}	0.02173	$\sigma_{C4-N7}\rightarrow\sigma^*_{C3-C4}$	< 0.50	1.51	1.57	1.35	1.55
		σ^*_{C4-C5}	0.02774	$\sigma_{C4-N7}\rightarrow\sigma^*_{C4-C5}$	0.59	< 0.50	0.62	0.63	0.60
		σ^*_{C8-O10}	0.00876	$\sigma_{C4-N7}\rightarrow\sigma^*_{C8-O10}$	14.83	3.49	3.28	3.29	3.24
σ_{C5-C6}	1.97364	σ^*_{C1-C6}	0.01363	$\sigma_{C5-C6}\rightarrow\sigma^*_{C1-C6}$	2.19	2.86	2.52	2.97	2.20
		σ^*_{C4-C5}	0.02774	$\sigma_{C5-C6}\rightarrow\sigma^*_{C4-C5}$	4.64	20.80	5.11	5.09	5.11
		σ^*_{C1-H23}	0.01344	$\sigma_{C5-C6}\rightarrow\sigma^*_{C1-H23}$	0.86	2.32	2.30	2.29	2.17
		σ^*_{C4-N7}	0.03575	$\sigma_{C5-C6}\rightarrow\sigma^*_{C4-N7}$	2.18	1.92	2.26	2.22	2.27
		σ^*_{C5-C9}	0.06643	$\sigma_{C5-C6}\rightarrow\sigma^*_{C5-C9}$	98.81	3.31	3.21	3.29	3.21
		σ^*_{C8-C9}	0.13462	$\sigma_{C5-C6}\rightarrow\sigma^*_{C8-C9}$	1.54	1.39	0.63	0.61	0.64
π_{C5-C6}	1.64203	π^*_{C1-C2}	0.31449	$\pi_{C5-C6}\rightarrow\pi^*_{C1-C2}$	16.04	20.23	16.12	< 0.50	13.59
		π^*_{C9-O11}	0.14210	$\pi_{C5-C6}\rightarrow\pi^*_{C9-O11}$	22.03	14.40	21.15	< 0.50	20.95
σ_{C5-C9}	1.97488	σ^*_{C5-C6}	0.02280	$\sigma_{C5-C9}\rightarrow\sigma^*_{C5-C6}$	4.58	3.74	3.10	3.30	3.09
		σ^*_{C1-C6}	0.01363	$\sigma_{C5-C9}\rightarrow\sigma^*_{C1-C6}$	1.54	1.40	1.54	1.38	1.35
		σ^*_{C4-C5}	0.02774	$\sigma_{C5-C9}\rightarrow\sigma^*_{C4-C5}$	1.86	2.86	1.85	1.87	1.85
		σ^*_{C4-N7}	0.03575	$\sigma_{C5-C9}\rightarrow\sigma^*_{C4-N7}$	1.01	1.03	1.02	1.02	1.03
σ_{N7-C8}	1.98397	$\sigma^*_{C12-N16}$	0.02168	$\sigma_{N7-C8}\rightarrow\sigma^*_{C12-N16}$	2.60	1.93	2.54	1.75	2.61
		σ^*_{C4-N7}	0.03575	$\sigma_{N7-C8}\rightarrow\sigma^*_{C4-N7}$	1.70	1.69	1.73	1.74	1.72
		σ^*_{C8-O10}	0.00876	$\sigma_{N7-C8}\rightarrow\sigma^*_{C8-O10}$	< 0.5	0.82	0.90	0.87	0.87
σ_{C8-C9}	1.97417	σ^*_{C5-C6}	0.02280	$\sigma_{N7-C12}\rightarrow\sigma^*_{C12-N16}$	5.29	4.88	4.27	4.21	4.25
		σ^*_{C8-O10}	0.00876	$\sigma_{N7-C12}\rightarrow\sigma^*_{C4-C5}$	2.24	< 0.5	0.95	0.96	0.97

Donor NBO (*i*)	ED(*i*), a.u. (X=H)	Acceptor NBO(*j*)	ED(*j*), a.u. (X=H)	Interaction type	E_2 / kcal mol^{-1}				
					X=H	X=CH_3	X=F	X=CN	X=NO_2
σ_{N7-C12}	1.98420	$\sigma^*_{C12-N16}$	0.02168	$\sigma_{N7-C12} \rightarrow \sigma^*_{C12-N16}$	1.97	1.54	1.89	1.30	1.88
		σ^*_{C4-C5}	0.02774	$\sigma_{N7-C12} \rightarrow \sigma^*_{C4-C5}$	0.84	1.17	0.83	0.80	0.80
		σ^*_{C4-N7}	0.03575	$\sigma_{N7-C12} \rightarrow \sigma^*_{C4-N7}$	1.94	2.00	1.98	1.98	1.99
		σ^*_{N7-C8}	0.08751	$\sigma_{N7-C12} \rightarrow \sigma^*_{N7-C8}$	1.85	2.21	1.53	1.52	1.52
		σ^*_{C8-C9}	0.13462	$\sigma_{N7-C12} \rightarrow \sigma^*_{C8-C9}$	0.80	0.76	0.79	0.77	0.77
		$\sigma^*_{N13-C14}$	0.03835	$\sigma_{N7-C12} \rightarrow \sigma^*_{N13-C14}$	0.74	1.12	1.12	1.00	1.14
$\sigma_{C12-N13}$	1.98380	σ^*_{C4-N7}	0.03575	$\sigma_{C12-N13} \rightarrow \sigma^*_{C4-N7}$	2.30	2.46	2.45	2.43	2.46
		$\sigma^*_{C12-N16}$	0.02168	$\sigma_{C12-N13} \rightarrow \sigma^*_{C12-N16}$	1.40	0.98	1.17	0.77	1.11
		$\sigma^*_{N13-C14}$	0.03835	$\sigma_{C12-N13} \rightarrow \sigma^*_{N13-C14}$	< 0.50	1.66	1.71	1.52	1.69
		$\sigma^*_{N13-H27}$	0.02547	$\sigma_{C12-N13} \rightarrow \sigma^*_{N13-H27}$	0.84	0.89	0.96	0.97	0.97
		$\sigma^*_{C14-N15}$	0.02169	$\sigma_{C12-N13} \rightarrow \sigma^*_{C14-N15}$	14.30	0.67	0.66	0.67	0.68
		$\sigma^*_{C14-C17}$	0.03287	$\sigma_{C12-N13} \rightarrow \sigma^*_{C14-C17}$	4.23	4.02	4.08	4.01	4.10
$\sigma_{C12-N16}$	1.98698	$\sigma^*_{C12-N13}$	0.03494	$\sigma_{C12-N16} \rightarrow \sigma^*_{C12-N13}$	1.37	1.30	1.44	1.20	1.39
		σ^*_{N7-C8}	0.08751	$\sigma_{C12-N16} \rightarrow \sigma^*_{N7-C8}$	2.22	2.56	1.80	1.79	1.81
		$\sigma^*_{N13-H27}$	0.02547	$\sigma_{C12-N16} \rightarrow \sigma^*_{N13-H27}$	0.92	2.16	2.30	2.31	2.32
		$\sigma^*_{C14-C17}$	0.03287	$\sigma_{C12-N16} \rightarrow \sigma^*_{C14-C17}$	0.53	0.57	0.58	0.57	0.58
$\pi_{C12-N16}$	1.86676	$\pi^*_{C14-N15}$	0.34975	$\pi_{C12-N16} \rightarrow \pi^*_{C14-N15}$	12.64	12.85	12.55	11.60	13.54
$\sigma_{N15-N16}$	1.97334	$\sigma^*_{C12-N13}$	0.03494	$\sigma_{N15-N16} \rightarrow \sigma^*_{C12-N13}$	1.22	0.89	1.00	0.83	0.96
		$\sigma^*_{N13-C14}$	0.03835	$\sigma_{N15-N16} \rightarrow \sigma^*_{N13-C14}$	0.51	1.21	1.23	1.07	1.19
		$\sigma^*_{C14-C17}$	0.03287	$\sigma_{N15-N16} \rightarrow \sigma^*_{C14-C17}$	5.02	4.68	4.62	4.47	4.61
$LP(1)_{N7}$	1.61989	$\pi^*_{C12-N16}$	0.39577	$LP(1)_{N7} \rightarrow \pi^*_{C12-N16}$	27.62	19.13	43.47	12.18	44.38
$LP(1)_{N13}$	1.58986	$\pi^*_{C12-N16}$	0.39577	$LP(1)_{N13} \rightarrow \pi^*_{C12-N16}$	6.81	21.53	50.89	13.07	51.20
		$\pi^*_{C14-N15}$	0.34975	$LP(1)_{N13} \rightarrow \pi^*_{C14-N15}$	1.64	44.79	43.68	36.21	43.32
$LP(1)_{N15}$	1.93991	$\sigma^*_{C12-N16}$	0.02168	$LP(1)_{N15} \rightarrow \sigma^*_{C12-N16}$	4.30	4.49	4.87	2.93	4.95
		$\sigma^*_{N13-C14}$	0.03835	$LP(1)_{N15} \rightarrow \sigma^*_{N13-C14}$	15.64	6.46	7.38	6.12	7.44
$LP(1)_{N16}$	1.93779	$\sigma^*_{C12-N13}$	0.03494	$LP(1)_{N16} \rightarrow \sigma^*_{C12-N13}$	7.90	5.93	7.38	5.84	7.32
		$\sigma^*_{C14-N15}$	0.02169	$LP(1)_{N16} \rightarrow \sigma^*_{C14-N15}$	20.83	4.81	4.83	4.89	4.91

According to the NBO analysis, the lone-pair of the N7 atom in the studied molecules has an exclusive *p*-character (100 %) and a low occupancy (1.61989 a.u.) resulting in greater stability interactions. As a result, for the $LP(1)_{N7} \rightarrow \pi^*_{C12-N16}$ interactions, electron donation to the $\pi^*_{C12-N16}$ antibonding orbital is very similar to the pure *p*-type lone-pair orbital (Table 4). The $LP(1)N_{13}$ lone-pair orbital has a lower energy (1.58986 a.u.) with a 99.98 % *p*-character. The other lone-pairs, $LP(1)_{N15}$ and $LP(1)_{N16}$ have the high occupation numbers of 1.93991 and 1.93779 a.u., respectively with *p*-character up to 60.93 and 60.48 %, correspondingly. The interaction of $LP(1)_{N7} \rightarrow \pi^*_{C12-N16}$ has higher stabilization energy of up to 43.47 kcal mol^{-1}. Similarly, the intramolecular hyperconjugative interactions of $LP(1)_{N15} \rightarrow \sigma^*_{N13-C14}$ and $LP(1)_{N16} \rightarrow \sigma^*_{C14-N15}$ have a stabilizing energy of up to 15.64 and 20.83 kcal mol^{-1}, respectively. Furthermore, with a stabilization energy of up to 7.90 kcal mol^{-1}, the interaction between the lone-pair $LP(1)_{N16}$ and the $\sigma^*_{C12-N13}$ antibonding orbitals results in intramolecular charge transfer, which contributes to the molecular system's stabilization.

4. Conclusion

Solvation and substituent effects of the electron-releasing/withdrawing groups on synthesized 1-(5-phenyl-4*H*-1,2,4-triazol-3-yl)indoline-2,3-dione and its derivatives (–CH_3, –F, –CN, –NO_2) studied at the B3LYP/6-311++G(d,p) level of theory in the gas phase and solvents (acetone, ethanol, and methanol). The energetic properties, dipole

moment, natural bond orbital analysis, frontier molecular orbitals, molecular electrostatic potential, and electric charges distribution of the studied compounds were considered with the same theoretical level. The obtained results indicate that 1,2,4-triazole derivatives can occur in both form **A** (non-linear) and form **B** (linear). The energetic results show that form **B** is more stable than the other form. The calculated dipole moment results show that the highest value is the nitro substituted of form **B** in acetone solvent, hence the dipole moment is increases from the gas phase to a more polar solvent. Frontier molecular orbital analysis finds that compound **5** ($X=NO_2$) in different media has high HOMO-LUMO energy gaps and is thus kinetically more stable. Chemical reactivity indices as follow: $NO_2 > CN > Cl > H > CH_3$ that predicts the lowest ($X=CH_3$) and highest ($X=NO_2$) activity for the considered compounds. The energy difference derived from HOMO-LUMO leads to intramolecular hyperconjugative interactions $\pi \rightarrow \pi^*$. The NBO analysis indicates intramolecular charge transfer allowing the molecule to stabilize.

References

[1] B. Namratha, S.L. Gaonkar, 1,2,4-triazoles: synthetic strategies and pharmacological profiles. Int. J. Pharm. Pharm. Sci. 6 (2014) 73.

[2] S. Nekkanti, R. Tokala, N. Shankaraiah, Targeting DNA minor groove by hybrid molecules as anticancer agents. Curr. Med. Chem. 24 (2017) 2887.

[3] S.A. El-Sebaey, Recent advances in 1,2,4-triazole scaffolds as antiviral agents. ChemistrySelect, 5 (2020) 11654.

[4] H.A.H. Elshemy, M.A. Zaki, E.I. Mohamed, S.I. Khan, P.F. Lamie, A multicomponent reaction to design antimalarial pyridyl-indole derivatives: Synthesis, biological activities and molecular docking. Bioorg. Chem. 97 (2020) 103673.

[5] K. Feng, C. Ni, L. Yu, W. Zhou, Synthesis and evaluation of acrylate resins suspending indole derivative structure in the side chain for marine antifouling. Colloids Surf B 184 (2019) 110518.

[6] V. Arjunan, G. Durg adevi, S. Mohan, An experimental and theoretical investigation on the structure, vibrations and reactivity properties of pharmacologically active compounds 3-acetylindole and indole-3-acetamide. J. Mol. Struct. 1210 (2020) 128012.

[7] N. Afshar, F. Hatamjafari, A. Shiroudi, K. Pourshamsian, A.R. Oliaey, Synthesis and characterization of some new indoline-based 1,2,4-triazole derivatives. Russ. J. Org. Chem. 56 (2020) 2153.

[8] N. Catozzi, M.G. Edwards, S.A. Raw, P. Wasnaire, R.J.K. Taylor, Synthesis of the Louisianin alkaloid family via a 1,2,4-triazine inverse-electron-demand Diels-Alder approach. J. Org. Chem. 74 (2009) 8343.

[9] E. Düğdü, Y. Ünver, D. Ünlüer, H. Tanak, K. Sancak, Y. Köysal, Ş. Işık, Synthesis, structural characterization and comparison of experimental and theoretical results by DFT level of molecular structure of 4-(4-methoxyphenethyl)-3,5-dimethyl-4H-1,2,4-triazole. Spectrochim. Acta A 108 (2013) 329.

[10] N. Özdemir, D. Türkpençe, Theoretical investigation of thione-thiol tautomerism, intermolecular double proton transfer reaction and hydrogen bonding interactions in 4-ethyl-5-(2-hydroxyphenyl)-2H-1,2,4-triazole-3(4H)-thione. Theor. Comput. Chem. 1025 (2013) 35.

[11] J.K. Shneine, Y.H. Alaraji, Chemistry of 1,2,4-triazole: a review article. Int. J. Sci. Res. 5 (2016) 1411.

[12] M.-X. Song, X.-Q. Deng, Recent developments on triazole nucleus in anticonvulsant compounds: a review. J. Enzyme Inhib. Med. Chem. 33 (2018) 453.

[13] M. Miar, A. Shiroudi, K. Pourshamsian, A.R. Oliaey, F. Hatamjafari, DFT study and NBO analysis of solvation/substituent effects of 3-phenylbenzo[d]thiazole-2(3H)-imine derivatives. J. Serb. Chem. Soc., 85 (2020) 1445.

[14] M.A. Johnson, G.M. Maggiora, Concepts and Application of Molecular Similarity, John Wiley Sons, New York, (1990).

[15] E. Yadav, M. Singh, P.N. Saxena, Structure-activity relationship of some type-II Pyrethroids: A study based on atomic charges, molecular electrostatic potential surfaces and molecular orbitals analysis. Natl. Acad. Sci. Lett. 37 (2014) 245.

[16] S. Chidangil, P.C. Mishra, Structure-activity relationship for some 2′,3′-

dideoxynucleoside anti-HIV drugs using molecular electrostatic potential mapping. J. Mol. Model. 3 (1997) 172.

[17] U. Sarkar, D.R. Roy, P.K. Chattaraj, R. Parthasarathi, J. Padmanabhan, V. Subramanian, A conceptual DFT approach towards analysing toxicity. J. Chem. Sci. 117, (2005) 599.

[18] C. Lee, W. Yang, R.G. Parr, Development of the Colle-Salvetti correlation-energy formula into a functional of the electron density. Phys. Rev. B 37 (1988) 785.

[19] A.D. Becke, Density-functional thermochemistry. III. The role of exact exchange. J. Chem. Phys. 98 (1993) 5648.

[20] J.K. Badenhoop, F. Weinhold, Natural steric analysis of internal rotation barriers. Int. J. Quantum Chem. 72 (1999) 269.

[21] P.v.R. Schleyer, C. Maerker, A. Dransfeld, H. Jiao, N.J.R.V.E. Hommes, Nucleus-independent chemical shifts: A simple and efficient aromaticity probe. J. Am. Chem. Soc. 118 (1996) 6317.

[22] P. Cysewski, An ab initio study on nucleic acid bases aromaticities. J. Mol. Struct. (Theochem) 714 (2005) 29

[23] S. Nigam, C. Majumder, S.K. Kulshreshtha, Theoretical study of aromaticity in inorganic tetramer clusters. J. Chem. Sci. 118 (2006) 575.

[24] P.v.R., Schleyer, M. Manoharan, Z.X. Wang, B. Kiran., H. Jiao, R. Puchta, N. Hommes, Dissected nucleus-independent chemical shift analysis of π-aromaticity and antiaromaticity. Org. Lett. 3 (2001) 2465.

[25] P.v.R. Schleyer, H. Jiao, B. Goldfuss, P.K. Freeman, Aromaticity and antiaromaticity in five-membered C4H4X ring systems: “classical” and “magnetic” concepts may not be “orthogonal”. Angew. Chem. Int. Ed. Engl. 34 (1995) 337.

[26] J. R. Cheeseman, G.W. Trucks, T.A. Keith, M.J. Frisch, A comparison of models for calculating nuclear magnetic resonance shielding tensors. J. Chem. Phys. 104 (1996) 5497.

[27] K. Wolinski, J.F. Hinton, P. Pulay, Efficient implementation of the gauge-independent atomic orbital method for NMR chemical shift calculations. J. Am. Chem. Soc. 112 (1990) 8251.

[28] M.J. Frisch, G.W. Trucks, H.B. Schlegel, G.E. Scuseria, M.A. Robb, J.R. Cheeseman, G. Scalmani, V. Barone, B. Mennucci, G.A. Petersson, et al., Gaussian 09, Revision B. 01; Gaussian: Wallingford, CT, 2009.

[29] M.W. Schmidt, K.K. Baldridge, J.A. Boatz, S.T. Elbert, M.S. Gordon, J.H. Jensen, S. Koseki, N. Matsunaga, K.A. Nguyen, S.J. Su, T.L. Windus, M. Dupuis, J.A. Montgomery, General atomic and molecular electronic structure system. J. Comput. Chem. 14 (1993) 1347.

[30] S. Miertuš, E. Scrocco, J. Tomasi, Electrostatic interaction of a solute with a continuum. A direct utilization of Ab initio molecular potentials for the prevision of solvent effects. Chem. Phys. 181, 55 (1981) 117.

[31] S. Miertuš, J. Tomasi, Approximate evaluations of the electrostatic free energy and internal energy changes in solution processes. Chem. Phys. 65 (1982) 239.

[32] M.T. Cancès, V. Mennucci, J. Tomasi, A new integral equation formalism for the polarizable continuum model: theoretical background and applications to isotropic and anisotropic dielectrics. J. Chem. Phys. 107 (1997) 3032.

[33] M. Alcolea Palafox, G. Tardajos, A. Guerrero-Martinez, V.K. Rastogi, D. Mishra, S.P. Ojha, W. Kiefer, FT-IR, FT-Raman spectra, density functional computations of the vibrational spectra and molecular geometry of biomolecule 5-aminouracil. Chem. Phys. 340 (2007) 17.

[34] A. Salimi Beni, M. Aazari, A. Najafi Chermahini, M. Zarandi, Density functional theory of tautomerism and water-assisted proton transfer of glycoluril. Russ. J. Phys. Chem. A 90 (2016) 1859.

[35] P.v.R. Schleyer, H. Jiao, What is aromaticity? Pure Appl. Chem. 68 (1996) 209.

[36] T.M. Krygowski, M. Cyranski, A. Ciesielski, B. Swirska, P. Leszczynski, Separation of the energetic and geometric contributions to aromaticity, 2. Analysis of the aromatic character of benzene rings in their various topological environments in the benzenoid hydrocarbons. J. Chem. Inf. Comput. Sci. 36 (1996) 1135.

[37] S. Xavier, S. Periandy, Spectroscopic (FT-IR, FT-Raman, UV and NMR) investigation

on 1-phenyl-2-nitropropene by quantum computational calculations. Spectrochim. Acta A 149 (2015) 216.

[38] Y. Ruiz-Morales, HOMO−LUMO gap as an index of molecular size and structure for polycyclic aromatic hydrocarbons (PAHs) and Asphaltenes: a theoretical study. I. J. Phys. Chem. A 106 (2002) 11283.

[39] E. Scrocco, J. Tomasi, Electronic molecular structure, reactivity and intermolecular forces: An Euristic interpretation by means of electrostatic molecular potentials. Adv. Quantum Chem. 11 (1979) 115.

[40] J.E. Carpenter, F. Weinhold, Analysis of the geometry of the hydroxymethyl radical by the “different hybrids for different spins” natural bond orbital procedure. J. Mol. Struct. (Theochem) 169 (1988) 41.